

# Self-assembled particle monolayers on polyelectrolyte multilayers: particle size effects on formation, structure, and optical properties

Jin Soo Ahn<sup>a</sup>, Paula T. Hammond<sup>b</sup>, Michael F. Rubner<sup>c</sup>, Ilsoon Lee<sup>a,\*</sup>

<sup>a</sup> Department of Chemical Engineering and Materials Science, 2527 Engineering Building,  
Michigan State University, East Lansing, MI 48824, USA

<sup>b</sup> Departments of Chemical Engineering, Massachusetts Institute of Technology, Cambridge, MA 02139, USA

<sup>c</sup> Departments of Materials Science and Engineering, Massachusetts Institute of Technology, Cambridge, MA 02139, USA

Received 9 August 2004; accepted 5 February 2005

Available online 14 March 2005

## Abstract

Monolayers of charged polystyrene latex particles ranging in size from 100 nm to 10  $\mu\text{m}$  were deposited on oppositely charged polyelectrolyte multilayers (PEMs) by electrostatic interactions and capillary forces. Ultrathin PEMs ( $\sim 30$  nm) formed on a glass slide provided an excellent underlying adhesive layer. As the sample surface was being dried, strong capillary forces between particles resulted in a unique pattern of particle monolayers (i.e., two-dimensional (2-D) particle aggregates). The resulting topographical structure of the coatings strongly influenced the transmission of visible light through the slides. The total and specular transmittances showed three different characteristics as a function of particle size: (1) anti-reflection, when the particle diameter ( $D_{\text{particle}}$ ) is around a quarter of the wavelength of the incident visible light ( $D_{\text{particle}} \sim \lambda_{\text{vis}}/4$ ), (2) diffraction, when the  $D_{\text{particle}}$  is equivalent to the wavelength of the incident beam ( $D_{\text{particle}} \sim \lambda_{\text{vis}}$ ), and (3) diffusive scattering when the  $D_{\text{particle}}$  is bigger than the wavelength of the incident beam ( $D_{\text{particle}} \sim \lambda_{\text{vis}}$ ). Additionally, for the first time, the monolayer coverage and fractal-dimension analyses have been reported over a wide range of particle sizes. Functional groups present in these coatings allow further customization via chemical modification.

© 2005 Elsevier B.V. All rights reserved.

**Keywords:** Polyelectrolyte multilayers; Optical properties; Particle size; Particle monolayer; Anti-reflection; Diffraction; Diffusive scattering

## 1. Introduction

Studies of colloidal particle assembly at surfaces have provided fundamental insight into colloidal behavior and aggregation, and suggested potential applications such as optical band gap materials and coatings. Ordered, three-dimensional (3-D) colloidal multilayers have been investigated as optical filters and photonic crystals [1–8]. Two-dimensional (2-D), colloidal assemblies have been investigated for applications including anti-reflection (AR) coatings [9], gratings [10], interferometers [11], photolithographic masks [12–14], and optical coatings [15–17]. Recent developments in 2-D assemblies include the positioning of particles on desired

surface regions [18–24] and incorporation of molecular and colloidal materials into spatial patterns [7,15,25].

Two-dimensional particle monolayers assembled on surfaces can be categorized as either densely close-packed or randomly dispersed. Densely close-packed particle monolayers have been fabricated using spin coating [26], Langmuir Blodgett (LB)-techniques [27], thin laminar flow liquid film [28], monolayer transfer [12], and electrophoretic deposition [29]. Although these methods have successfully produced hexagonally packed particle arrays, they were tedious to perform or required specific devices; in addition, long-range ordering has been a problem for their practical applications. Evaporation methods are simple and widely used in making densely packed particle monolayers [30], but the size of ordered regions produced has been limited. To achieve close packing over a larger area, additional control is required (e.g., tilting samples in the evaporation process [13]).

\* Corresponding author. Tel.: +1 517 355 9291; fax: +1 517 432 1105.  
E-mail address: leeil@egr.msu.edu (I. Lee).

On the other hand, fabrication of randomly dispersed monolayers is relatively easy and does not require special devices [9,31–36]. Also, random particle monolayer coatings can avoid ‘Bragg Diffraction’, which must be minimized for certain coating applications (e.g., diffusive scattering films). Among various random deposition methods, electrostatic deposition using polyelectrolyte multilayers (PEMs) as an ultrathin adhesive layer has advantages of being simple to perform, cost-effective, and environmentally friendly. PEMs are formed in the layer-by-layer assembly process, which consists of the sequential alternating immersion of a substrate into polycation and polyanion solutions to construct a nanostructured ultrathin film. Charged particles can then be deposited via electrostatic interactions to form monolayers atop the PEM.

Layer-by-layer electrostatic assembly of PEMs, originally developed by Decher [37,38], has been widely studied because of its versatility and potential applications. Fabrication of nanostructured PEM films is simple and can be successfully achieved without the need for a clean-lab facility [39–41]. The PEMs can be formed on flat, curved, and even spherical surfaces (e.g., a colloidal particle) [7,42,43]. Additionally, PEMs contain multiple functional groups that can serve as molecular templates for further customization. Dendrimers [44–47], proteins [48–50], cells [51], and inorganic nanoparticles [52–61] have been co-assembled into PEM.

The properties of randomly dispersed monolayers depend on particle dispersion and clustering tendencies. Random-close-packed (RCP) particle monolayers contain branch-like structures of interconnected and/or hexagonally packed particles. Lateral capillary forces and convective flow of solvent between particles help form ordered regions during solvent evaporation [30,62,63]. Hattori demonstrated that random monolayers of silica and polymeric nanoparticles ( $D_{\text{particle}} \sim 1/4\lambda$ ) yield an AR coating effect [9]. The structure and optical properties of the particle coatings were controlled by electrostatic repulsions and attractive capillary forces [15,34].

While the optical properties of colloidal multilayers and close-packed monolayers have been extensively studied, those of randomly adsorbed or RCP monolayers have not. In this study, we systematically investigated RCP monolayers produced by electrostatically adsorbing PS particles between 100 nm and 10  $\mu\text{m}$  in diameter on PEM-coated glass slides. The surface coverage and fractal dimensions of the RCP monolayers were measured using image analysis, and the optical properties were studied using both total and specular transmittance. The possibility of modeling RCP monolayers based on the 2-D coverage and fractal dimension analysis using a box-count method [64] was also considered.

## 2. Experimental procedures

Poly(diallyldimethylammonium chloride) (PDAC) and sulfated poly(styrene) (SPS) were purchased from Aldrich.

Average molecular weights of PDAC and SPS were  $\sim 100,000$ – $200,000$  and  $70,000$ , respectively. Microscope glass slides were ordered from Corning and used as transparent substrates for PEMs and particle coatings. All aqueous solutions in the processes were prepared using deionized (DI) water ( $>18.1\text{ M}\Omega$ ) supplied by a Barnstead Nanopure Diamond-UV purification unit equipped with a UV source and final  $0.2\ \mu\text{m}$  filter. All procedures were done at room temperature.

Glass slides were first cleaned twice in an ultrasonic unit, first with a commercially available detergent (Alconox, Alconox Inc.) and then without. Slides were dried under a  $\text{N}_2$  gas stream and then treated with oxygen plasma for 10 min at 150 mTorr vacuum to activate negative surface charges on the glass.

Aqueous polyelectrolyte solutions were prepared containing either 20 mM PDAC or 10 mM SPS in 0.1 M NaCl. PDAC/SPS bilayers were then deposited by sequential immersion of the glass slides into the two solutions using a Microm DS 50 Slide Stainer purchased from Richard-Allan Scientific. PDAC was deposited first, because its positively charged amine groups bind to the negatively charged hydroxyl groups of glass. In each step, the slides were immersed in a polyelectrolyte solution for 20 min, followed by two 5 min rinses in DI water. After each PDAC/SPS bilayer was deposited, the slides were immersed in an ultrasonic bath for 1 min to remove loosely attached polyelectrolyte. This sequence was repeated until (PDAC/SPS)<sub>10.5</sub> bilayers were formed. (PDAC/SPS)<sub>10.5</sub> bilayers have a positive PDAC top layer which is needed to electrostatically bind the negatively charged PS particles. Substrates were finally dried under a  $\text{N}_2$  gas stream and stored for particle coating. The surfactant-free sulfate-functionalized and carboxylic-acid-functionalized PS particles were obtained from Interfacial Dynamics Corp., and Polysciences Inc., respectively. Size-distribution and surface-charge density information obtained from the manufacturers is shown in Table 1.

To bind PS particles to the PEM, a 0.5 wt.% colloidal solution was gently dropped on the glass slide. After 1 h incubation, the particle-coated substrates were washed carefully with deionized water and dried under a  $\text{N}_2$  stream. Microscopic images of the coatings were obtained using a Nikon Eclipse ME600 optical microscope and a JEOL 6400V scanning electron microscope (SEM) with a LaB6 emitter. The degree of surface coverage was determined by counting particles in a given area. Coverage measurements were repeated several times in both particle-rich and particle-poor regions. Data were reported as average standard deviation values.

Microscopic images were further investigated by fractal analysis using a 2-D box-counting method [64]. All monolayer images were scaled to have the same particle sizes, and each particle was considered as a single point. The maximum number of boxes was 4096. Boxes were counted manually and plotted on logarithmic-scale graph. Fractal dimensions were calculated using a least squares regression method. A

Table 1  
Details of particles used and their monolayers

Particle size ( $\mu\text{m}$ )	Size distribution diameter $\pm$ S.D. ( $\mu\text{m}$ )	Surface functional group	Surface charge density ( $\mu\text{eq/g}$ )	Monolayer coverage by particles $\pm$ S.D. (%)	Fractal dimension, $D_f$
0.14	$0.14 \pm 0.003$	Sulfate	$3.4^b$	$32.6 \pm 1.8$	1.778
0.2	$0.194 \pm 0.009$	Carboxylate	100–200 <sup>a</sup>	N/A <sup>c</sup>	N/A <sup>c</sup>
0.5	$0.477 \pm 0.01$	Carboxylate	100–200 <sup>a</sup>	$40.4 \pm 9.9$	1.799
1	$1.0 \pm 0.047$	Sulfate	$83.9^b$	$39.4 \pm 0.8$	1.804
2	$1.96 \pm 0.06$	Carboxylate	100–200 <sup>a</sup>	$39.4 \pm 1.4$	1.800
3	$3.00 \pm 1.44$	Carboxylate	100–200 <sup>a</sup>	$54.2 \pm 1.7$	1.828
4	$4.0 \pm 0.14$	Sulfate	$0.8^b$	$59.4 \pm 2.9$	1.848
5	$4.9 \pm 0.275$	Sulfate	$0.5^b$	$47.4 \pm 6.3$	1.846
8	$7.9 \pm 0.845$	Sulfate	$0.4^b$	$67.4 \pm 18.7$	1.826
10	$9.6 \pm 0.710$	Sulfate	$1^b$	$65.1 \pm 19.7$	1.835

<sup>a</sup> Approximation from the Polysciences Inc.

<sup>b</sup> Approximations from the Interfacial Dynamics Corp.

<sup>c</sup> 0.2  $\mu\text{m}$  particles resulted in local bilayers in the entire region. Surface monolayer coverage is not applicable.

UV/VIS/NIR Spectrometer Lambda 900 (Perkin-Elmer) was used to study the optical properties of the samples. Two detectors, a photomultiplier tube (PMT) and an integrating sphere (IS), were used for specular and total transmittance characterization, respectively. All spectroscopic spectra of the samples were referenced against air, without a substrate.

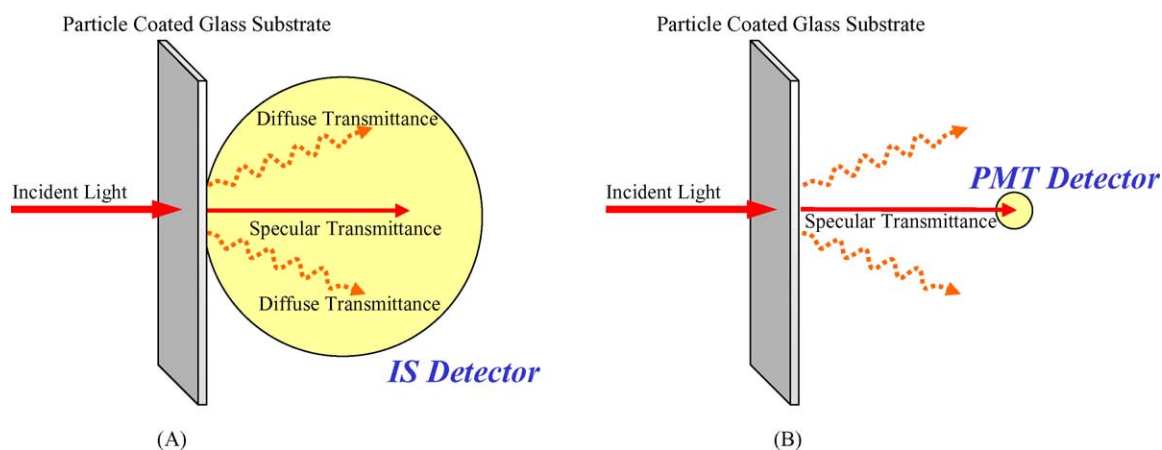
Scheme 1 illustrates the difference in measurement principle between the PMT and IS detectors. The IS detector collects all light passing through the substrate regardless of the back scattering angle (total transmittance), while the PMT detector only captures light transmitted in the same direction as the incident light (specular transmittance). Transmittance spectra from both detectors were averaged at 400–800 nm wavelength range to compare the size effects on scattering (averaged total and specular transmittances). The total transmittance spectrum of every particle monolayer is not reported, because there was little change in light intensity with wavelength. However, all specular transmittance spectra are presented and categorized into three groups, depending on the optical behavior.

### 3. Results and discussion

The thickness of (PDAC/SPS)<sub>10.5</sub> films was previously reported to be around 30 nm [51]. The stability of particle coatings was found to depend on the thickness of PEMs since a single cationic polyelectrolyte layer was not sufficient to strongly hold larger ionic PS particles more than 3  $\mu\text{m}$ . In addition, the PEM adhesive layers used in the work did not significantly affect the transmission of light in the visible light regime.

#### 3.1. Formation of particle monolayers on PEMs

Fig. 1 shows the SEM and optical microscope images of the particle monolayers assembled on the (PDAC/SPS)<sub>10.5</sub>-coated glass slides. A monolayer of the negatively charged particles strongly adhered to the positively charged surface of the PEMs. However, particle multilayers that adhered to the initial adsorbed particle monolayer by the force of gravity were easily rinsed away since no specific interactions like



Scheme 1. Measurement schematics for the transmittance depending on detector types. (A) Total transmittance. (B) Specular transmittance. The integrating sphere (IS) detector captures all the light transmitted through the substrates resulting in total transmittance. The photomultiplier tube (PMT) detector only captures light transmitted in the same direction as the incident light resulting in specular transmittance.

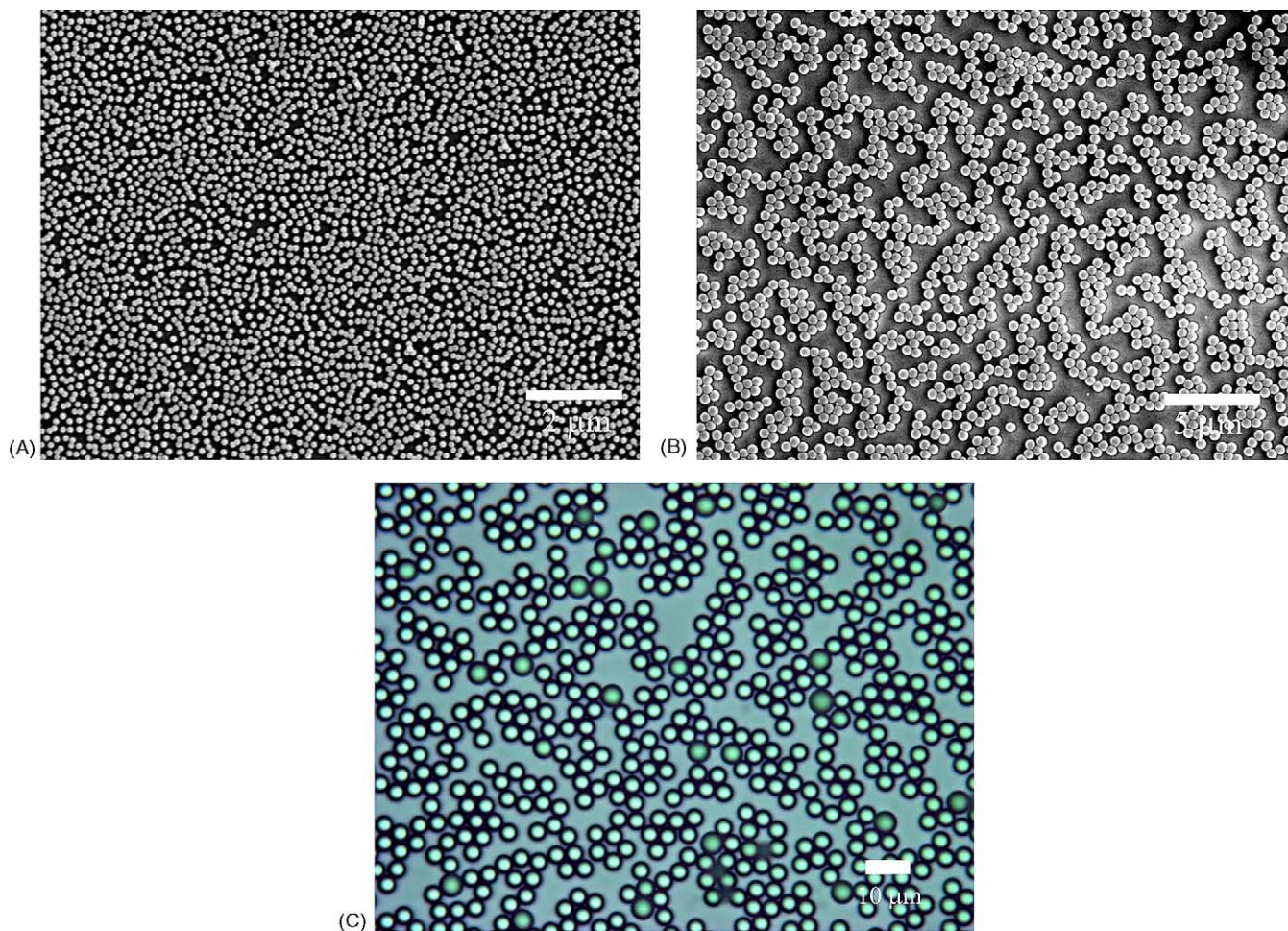


Fig. 1. SEM and optical microscopic images of self-assembled monolayers of functional polystyrene particles on PEMs. Depending on the size of particles, monolayers result in randomly adsorbed particles or random-close-packed clusters. (A) SEM image of 140 nm sized particles. (B) SEM image of 500 nm sized particles. (C) Optical microscopic image of 4  $\mu\text{m}$  sized particles.

electrostatic interaction were introduced between the same charged multilayered particles. It was observed under the optical microscope that before the evaporation of solvent particles (larger than 5  $\mu\text{m}$ ) on the substrate moved around even with the strong attractive force to the surface. Once the solvent was completely dried, all samples resulted in the irreversible 2-D particle aggregates on the PEMs.

Particles 140 nm in diameter formed monolayers in which particles were well dispersed on the PEM surface, with interactions between particles being limited to small, 2-D clusters and chains (Fig. 1A). Microspheres (0.5–10  $\mu\text{m}$ ) formed monolayers having larger 2-D clusters with fractal-like properties (Fig. 1B and C). Two hundred nanometers sized particles did not form a complete monolayer; instead they formed local bilayers in a wide area of samples. It may require a more vigorous washing step to prepare complete monolayers.

In the beginning of functional particle deposition in aqueous solution, the negatively charged particles were attracted to the positively charged PEM surfaces until the available PEM surfaces were fully occupied. Then, during the sample drying step when the water level became comparable to the

size of adsorbed particles, a rearrangement of adsorbed particles started to occur, resulting in uniquely self-assembled monolayer patterns on the PEM-coated glass slides, as shown in Fig. 1. During the rearrangement of adsorbed particles near or on the PEM-substrate, two conflicting forces, repulsive and attractive forces, compete to determine the pattern of the self-assembled particle monolayers. It is not simple to describe in detail how exactly all the factors contribute to the attractive and repulsive force, but in this work mainly capillary attractive forces and electrostatic repulsive forces are considered. The repulsive forces between particles adsorbed onto PEM surfaces are mainly due to the same particle charges. The attractive forces are because of capillary forces stimulated from the menisci of water formed around the particles [22]. The low density of sulfate groups makes the surface of the particle relatively more hydrophobic than the high density of carboxylate groups (see Table 1). However, in the case of larger particles the two different types of functional groups did not significantly affect the final fractal structures of 2-D aggregated particle monolayers. This is because only attractive capillary forces can be generated between the same

type of particles whatever they are hydrophilic or hydrophobic surfaces. The capillary force is known to be two orders of magnitude higher than the electrostatic repulsion force for micron sized particles [22]. However, in the case of the smallest particles (140 nm), the capillary force did not play a role in particle rearrangement (see Fig. 1A). Unlike the larger particles, the smallest particle monolayers remained almost the same without rearrangement during the drying step. Repulsive forces hinder the packing of two-dimensional particles while attractive forces help the packing of particles by the convective transport of particles toward the close packed region. We believe that the attractive forces were smaller than the repulsive forces in the case of 140 nm nanospheres, this results in particles that are relatively isolated from each other [66]. This conclusion is supported by the fact that particle closed packing can be obtained in the same system by reducing electrostatic repulsive forces between particles using surfactant charge screening [19]. For particles larger than 0.5  $\mu\text{m}$ , the attractive forces were dominant at the last stage of drying, resulting in the RCP particle monolayers.

Quantitative analyses of capillary force between colloidal particles and electrostatic repulsive are complicated, especially in a multi-particle system, and affected by not only the size of particle but also chemical composition of particle surface, charge distributions, and surface morphology. The detailed quantitative studies remain as future work.

### 3.2. Structure of self-assembled particle monolayers on PEMs

Table 1 shows physical data of the particles used in this work and monolayer coverage characterized by direct particle counting. The fifth column of Table 1 shows the calculated particle coverage, ranging at 32.6–67.4%, from the microscopic images. The coverage of the particle monolayers generally increased with an increase in the size of the particles. We believe that this reflects the dependency of capillary force on the particle size, which is the main contribution of the structural rearrangement of particle monolayers during the drying step. However, the surface coverage did not reach a theoretical maximum in this work. The calculated maximum surface coverage by spherical objects is 90.69% when they are hexagonally packed. Electrostatic monolayers do not form hexagonally packed monolayers due to the strong repulsive electrostatic forces, as reported elsewhere [19].

Surface coverage mainly relates with the dynamic actions of capillary and electrostatic forces, and also possibly with other factors such as gravitational force and hydrodynamic interactions [67]. Serizawa et al. [33] demonstrated the controllability of nanoparticles surface coverage using salt concentration, indicating the importance of hydrodynamic interactions on surface coverage. However, we experimentally observed that the net attractive forces inducing 2-D particle aggregates were found to be proportional to the particle size.

When particles are strongly attached to the substrate, the diffusion process or surface migration of particles is hindered

and there is a limit for coverage known as the jamming limit of random sequential adsorption (RSA) [68,69]. 54.7% is in good agreement for the maximum coverage by this model [68,69]. However, RCP monolayers with particles greater than 2  $\mu\text{m}$  have coverage greater than this limit (see Table 1). This means there is movement and diffusion of particles during the deposition and evaporation processes, which allow the particles to surpass the jamming limit. It also implies that the RSA model cannot explain the formation mechanism of RCP monolayer, though it resembles the initial stage of a RCP monolayer before evaporation of the solvent.

The structure of colloidal aggregates formed in this process is a fingerprint of the kinetics and mechanism of aggregation. Simple aggregation models and real aggregation processes frequently lead to fractal structures that can be described in terms of fractal geometry concepts [70]. Fractal geometry, also known as the fractal dimension, enables us to relate certain aggregates to a proper kinetic and growth mechanism model [71]. In two-dimensional analysis, the fractal dimension has a value of between one and two. When fractal geometry completely fills a certain area of the surface, the fractal dimension reaches the maximum value of 2.

We calculated the fractal dimensions of our samples in an effort to find a proper model to explain the uniquely self-arranged particle monolayers on PEMs. The last column of Table 1 presents the calculated 2-D fractal dimensions,  $D_f$ , of each sample. Fractal dimensions of RCP monolayers range from 1.778 to 1.848. The aggregation shape of the RCP model closely resembles that of cluster-cluster aggregation by primary clusters. There are two different models for this type of aggregation, ‘reaction-limited cluster-cluster aggregation’ (RLCCA) and ‘diffusion-limited cluster-cluster aggregation’ (DLCCA) [72].

When an aggregation rate is solely affected by the diffusion and collision of particles, the DLCCA model can explain the process [73]. On the other hand, an aggregation rate is limited by a residual energy barrier of bond formation, requiring higher collision energy; the RLCCA model applies [74]. When there is a residual repulsive force between colliding particles, generally RLCCA model better explains the dynamic aggregation phenomena. In addition, it is known that the fractal dimension of RLCCA is higher than that of DLCCA [72]. A high fractal dimension of RCP monolayer indicates its close relationship with the RLCCA model. However, relating the aggregate structure on PEM to a specific growth mechanism is not fully understood in this paper, and further theoretical and experimental research is required.

### 3.3. Light transmittance of particle-coated samples

Fig. 2A shows the average total transmittance of the samples at the visible light range (400–800 nm), which was measured using a UV–vis spectrometer equipped with an IS detector. The average total transmittances, ranging from 90.06 to 94.12%, remained very high and are comparable to the values of a pure glass slide. The average transmittance of a pure

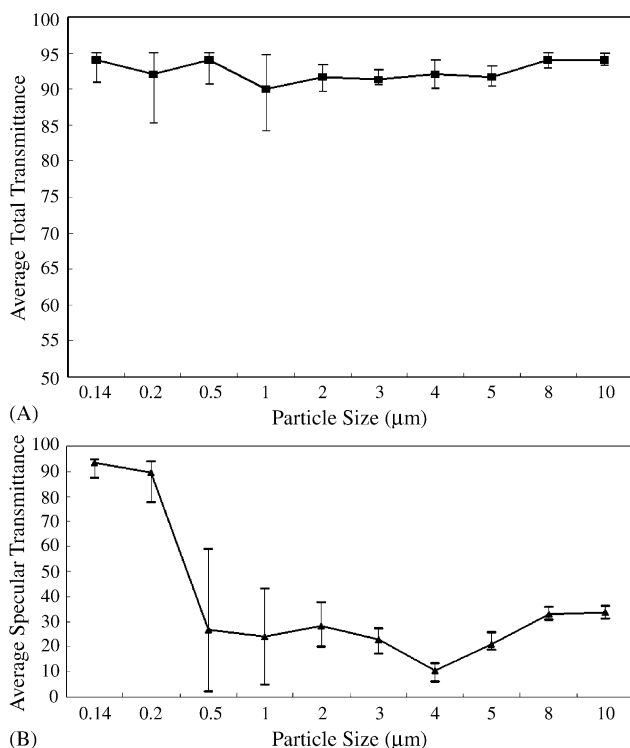


Fig. 2. Averaged transmittance measured using an IS and a PMT detectors with a wavelength range of 400–800 nm. (A) Average total transmittance measured using an IS detector. The IS detector captures all light transmitted through the sample films resulting in total transmittance. (B) Average specular transmittance from a PMT detector. The PMT detector only captures light that is not scattered by the substrate resulting in specular transmittance.

glass slide measured by the same IS detector was 91.86% at the same range of wavelengths. According to the total transmittance of the samples, reflection or absorption by the coated polystyrene particle monolayer has been small. Also, there is no significant particle size effect on the observed total transmittance. This implies that the particle monolayer coatings are suitable for optical coatings with little light loss by backscattering.

Fig. 2B shows the averaged specular transmittance measured using a PMT detector. The specular transmittance varies with the size of particle. A decrease in the specular transmittance compared to the observed total transmittance of the same sample indicated that some portion of incident light did not reach the detecting point because of a ‘scattering’ event. Monolayers of particles bigger than 0.5 μm yielded an ‘apparent scattering’ event when incident visible light passed through the particle coated glass slides. Apparent scattering happens when the size of the scattering particle is equal to or greater than the wavelength of incident radiation [75]. Particle coated glass slides with 140 and 200 nm sized particles did not exhibit significant scattering events. The samples looked either transparent without scattering events or translucent with those scattering events, depending on the size of particles.

Fig. 3 shows the specular transmittance spectra from the UV–vis spectroscopy experiment using a PMT detec-

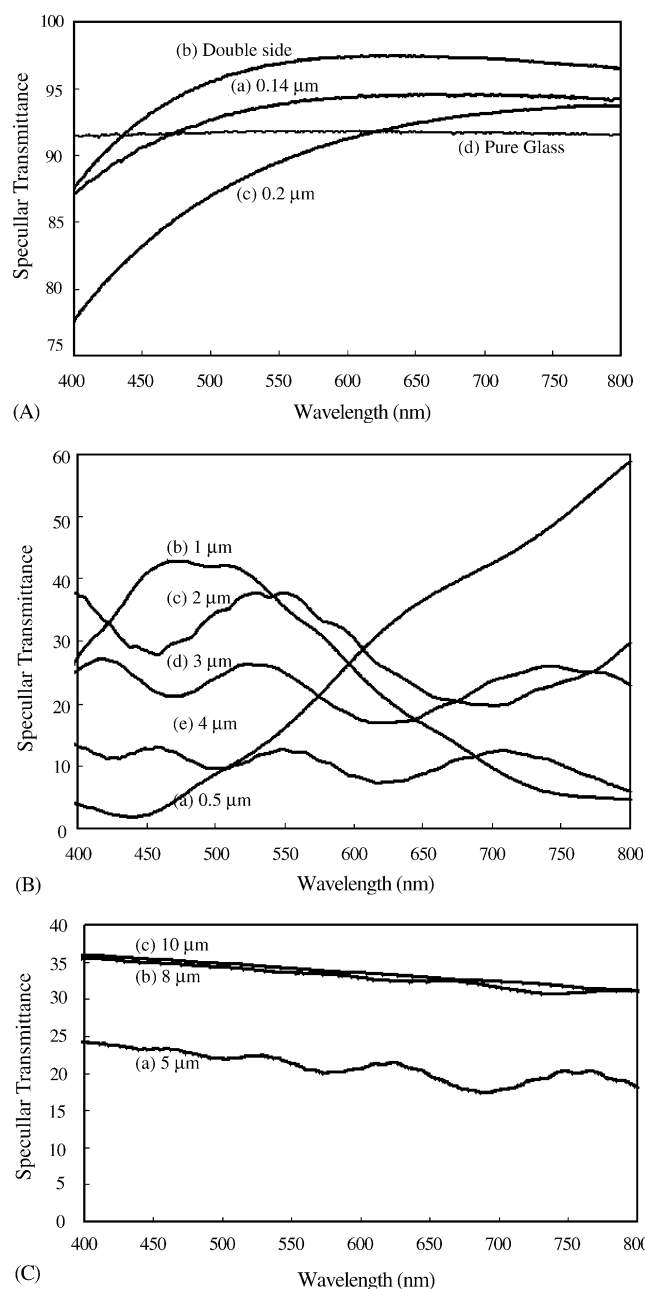


Fig. 3. Specular transmittance spectra measured using a PMT detector. Depending on the size of particles, optical properties were categorized into three main groups: (A) anti-reflective, (B) diffractive, and (C) diffusive scattering behaviors.

tor, which was not averaged. There are three main behaviors observed which are dependent on the particle size: anti-reflection behavior for the particles ranging in size from 0.14 to 0.2 μm (Fig. 3A), diffraction for the particles ranging in size from 0.5 to 4 μm (Fig. 3B), and diffusive scattering for the particles ranging in size from 5 to 10 μm (Fig. 3C).

Fig. 3A shows the transmittance spectra using a PMT detector in the visible light range, 400–800 nm. Particles with diameters of 140 and 200 nm have an AR behavior and exhibit an enhanced transmittance that is greater than that of a pure

glass over certain parts of the light range. Glass slides coated with particles on both sides have a higher transmittance than those coated on a single side. The maximum value of transmittance for this particle size was measured to be 97.52% at a wavelength of 635 nm, which is much higher than that of the pure glass slide (ca. 92%).

To be an AR coating, the designed film should satisfy two conditions [76]. The thickness of the AR coating must be a quarter of the incident wavelength and  $n_c = (n_a n_s)^{1/2}$ , where  $n_c$ ,  $n_a$ , and  $n_s$  are the refractive indices of the coating, air, and substrate, respectively. Anti-reflective behavior is due to the destructive interference between reflected light from the top surface of AR coating and from the reflected light of the interface between the AR coating and substrate. Also,  $n_c$  must have a value in between  $n_a$  and  $n_s$  so that the change in refractive indices of the media is gradual and reduces the amount of light reflecting backwards from the substrate.

The particle coatings that we produced with 140 and 200 nanometers sized particles satisfy both conditions for an AR coating. The thickness of these monolayers is directly decided by the diameters of the particles, which is around a quarter of the visible light wavelengths. Refractive indices of air, glass, and polystyrene particles are generally 1, 1.5, and 1.59 (data from Interfacial Dynamics Corp.), respectively. Due to the random deposition of particles, the monolayer has many pores between polystyrene particles that are filled with air. The monolayer has a refractive index somewhere in between that of air and polystyrene particles. As illustrated by Hattori [9], this approach to forming an AR coating does not require a high vacuum that is common in many AR coating processes. This process is more cost-effective when compared to phase separation or selective dissolution approaches [77] and simpler than vapor deposition or sputtering approaches [78,79]. However, it should be noted that inorganic nanoparticles on PEM would not present an AR behavior because the refractive index of inorganic nanoparticles is much higher than that of glass slide. The Rubner group has developed the AR coating without using nanoparticles to achieve a 99% transmission after the spinodal decomposition of a weak PEM system [80]. Because the coverage of AR monolayer, shown in the Table 1, is not high, it is expected that the total transmission will increase as the particle packing density increases [19].

Fig. 3B shows the oscillating specular transmittance spectra from particles with 0.5, 1, 2, 3, and 4  $\mu\text{m}$ . In the late sixties Krieger and O'Neill [75] demonstrated that monodispersed latex particles exhibited diffraction in both colloidal solution and dry particle layers. Since the incident light impinges the monolayer surface vertically, and particle structure is not fully ordered, Bragg diffraction is not arranged to explain this diffractive pattern. Instead, we believe this diffraction event can be categorized into Fraunhofer diffraction, which occurs when light propagates through an individual aperture or translucent screen [76]. This is supported by the fact that there is a typical airy disc created by a circular aperture when the laser from a laser pointer is shined through the samples. However, this airy disc pattern is unclear be-

cause the self-assembled particle monolayers on PEMs are RCP structures. Maxima and minima in the spectra represent the change in intensity with the change in the wavelength of incident monochromatic light.

Interesting results from the diffracted transmittance spectra are obtained for monolayers made from 0.5 to 1  $\mu\text{m}$  sized particles. A 0.5  $\mu\text{m}$  sized particle monolayer completely scatters blue light but transmits about 58% of incident red light. To the contrary, a 1  $\mu\text{m}$  sized particle monolayer scatters almost all incident red lights but passes 42% of incident blue light. By simply changing the size of the particles a particle monolayer can selectively block a specific wavelength.

Current studies on the selective transmission of incident light by diffraction have focused on 3-D colloidal crystals. In this case, sharp peaks at specific wavelengths are exhibited due to the Bragg diffraction through the ordered arrays. Selectivity in the transmission of light in narrow wavelength regions is useful in diffractive components of optical filters or in grating applications [2]. Different from ordered aggregations, RCP monolayers produce broad peaks that are unique in their diffraction through 2-D or 3-D multilayers.

While the details of this diffraction mechanism need to be further studied, we expect that there may be other potential applications in which this broad selective transmission can be very useful. We can further tune the optical selectivity using commercially available fluorescent particles [81]. Additionally, we can control these broad peaks using mixed or polydispersed particle monolayers.

Fig. 3C shows the specular transmittance spectra using a PMT detector from particles with diameters of 5, 8, and 10  $\mu\text{m}$ . This group exhibits uniform diffusive scattering of incident light. The transmitted light reaching the PMT detector shows a uniform intensity along with the wavelengths. The specular transmittance was decreased when compared to the total transmittance. This means that there happened to be a scattering event that changed the direction of the incident light. Optical coatings of the particle monolayers in this group transmitted diffraction free and uniform light. Once again, it is noted that the total transmittance measured using an IS detector remained almost the same regardless of the particle size. The transmitted light, through the self-assembled monolayers on PEM-coated glass slides, were scattered or diffracted differently depending on the topological surface structures controlled by the size of particles.

### 3.4. Conclusions

We have studied the functional PS particle size effects on the formations, structures, and optical properties of the uniquely self-assembled particle monolayers on PEM-coated glass slides. The particles formed RCP particle monolayers that deposited on the substrate by electrostatic attraction forces and then rearranged by capillary forces among the attached monolayer particles. Compared to other particle deposition approaches, the overall procedure used in this work was very simple, cost-effective, and environmentally

friendly. The formation and structure of the self-assembled particle monolayers (i.e., RCP particle monolayers) was analyzed using surface particle coverage and fractal dimension analysis. The optical properties of the self-assembled particle monolayers measured using two different detectors showed very interesting particle size dependencies. Even though the apparent changes dependent on particle size could be identified with the bare eye, the total transmittance, measured using an IS detector, remained unchanged and conversely the specular transmittance, measured using a PMT detector, changed considerably. No significant reflection or absorption by the coated monolayer has been found. This indicates that the incident visible light optically interacts with the particle monolayers through optical interference, diffraction, and/or scattering events. Three main optical characteristics as a ratio of particle diameter versus wavelength of incident visible light ( $D/\lambda$ ) are the following: (a) anti-reflection (when  $D/\lambda \sim 0.25$ ), (b) diffraction (when  $D/\lambda \sim 1$ ), and (c) diffusive scattering (when,  $D/\lambda > 1$ ). These functional and topographically structured surfaces can be further used as templates for selective and non-selective metal plating [82], cell adhesion [83], and quantum dot deposition [7].

## Acknowledgments

The analytical support provided through the Surface Characterization Facility in the Composite Materials and Structures Center at Michigan State University (MSU) is gratefully acknowledged. This work was funded by the Intramural Research Grant Program, the Center for Fundamental Materials Research at MSU, also by the Michigan Technology Tri-Corridor fund. Also, this work was supported in part by Hitachi Chemical, Co., Ltd., the MIT Microphotonics Research Center, and the Center for Materials Science and Engineering at the Massachusetts Institute of Technology.

## References

- [1] P. Jiang, J.F. Bertone, K.S. Hwang, V.L. Colvin, *Chem. Mater.* 11 (1999) 2132–2140.
- [2] S.H. Park, Y. Xia, *Langmuir* 15 (1999) 266–273.
- [3] A. Rogach, A. Susha, F. Caruso, G. Sukhorukov, A. Kornowski, S. Kershaw, H. Mohwald, A. Eychmuller, H. Weller, *Adv. Mater. (Weinheim, Germany)* 12 (2000) 333–337.
- [4] Y. Xia, B. Gates, Y. Yin, Y. Lu, *Adv. Mater. (Weinheim, Germany)* 12 (2000) 693–713.
- [5] C.-A. Fustin, G. Glasser, H.W. Spiess, U. Jonas, *Adv. Mater. (Weinheim, Germany)* 15 (2003) 1025–1028.
- [6] C. Lopez, *Adv. Mater. (Weinheim, Germany)* 15 (2003) 1679–1704.
- [7] D. Wang, A.L. Rogach, F. Caruso, *Chem. Mater.* 15 (2003) 2724–2729.
- [8] Y. Zhao, K. Wostyn, G. de Schaezen, K. Clays, L. Hellemans, A. Persoons, M. Szekeres, R.A. Schoonheydt, *Appl. Phys. Lett.* 82 (2003) 3764–3766.
- [9] H. Hattori, *Adv. Mater. (Weinheim, Germany)* 13 (2001) 51–54.
- [10] A. Kumar, G.M. Whitesides, *Sci., New Ser.* 263 (1994) 60–62.
- [11] J.M. Burch, *Nature* 171 (1953) 889–890.
- [12] F. Burmeister, C. Schaeffle, T. Matthes, M. Boehmisch, J. Boneberg, P. Leiderer, *Langmuir* 13 (1997) 2983–2987.
- [13] F. Burmeister, C. Schaeffle, B. Keilhofer, C. Bechinger, J. Boneberg, P. Leiderer, *Chem. Eng. Technol.* 21 (1998) 761–763.
- [14] M.-H. Wu, G.M. Whitesides, *Appl. Phys. Lett.* 78 (2001) 2273–2275.
- [15] H. Takei, *J. Vac. Sci. Technol., B: Microelectron. Nanometer Struct.* 17 (1999) 1906–1911.
- [16] M.T. Crisp, N.A. Kotov, *Nano Lett.* 3 (2003) 173–177.
- [17] P.T. Miclea, A.S. Susha, Z. Liang, F. Caruso, C.M.S. Torres, S.G. Romanov, *Appl. Phys. Lett.* 84 (2004) 3690.
- [18] J. Aizenberg, P.V. Braun, P. Wiltzius, *Phys. Rev. Lett.* 84 (2000) 2997–3000.
- [19] K.M. Chen, X. Jiang, L.C. Kimerling, P.T. Hammond, *Langmuir* 16 (2000) 7825–7834.
- [20] Y. Yin, Y. Lu, Y. Xia, *J. Mater. Chem.* 11 (2001) 987–989.
- [21] V. Brisson, R.D. Tilton, *Biotechnol. Bioeng.* 77 (2002) 290–295.
- [22] I. Lee, H. Zheng, M.F. Rubner, P.T. Hammond, *Adv. Mater. (Weinheim, Germany)* 14 (2002) 572–577.
- [23] Y. Masuda, M. Itoh, T. Yonezawa, K. Koumoto, *Langmuir* 18 (2002) 4155–4159.
- [24] H. Zheng, I. Lee, M.F. Rubner, P.T. Hammond, *Adv. Mater. (Weinheim, Germany)* 14 (2002) 569–572.
- [25] I. Lee, P.T. Hammond, M.F. Rubner, *Chem. Mater.* 15 (2003) 4583–4589.
- [26] F.-K. Liu, Y.-C. Chang, F.-H. Ko, T.-C. Chu, B.-T. Dai, *Microelectron. Eng.* 67–68 (2003) 702–709.
- [27] A.S. Dimitrov, K. Nagayama, *Langmuir* 12 (1996) 1303–1311.
- [28] G. Picard, I. Nevernov, D. Alliata, L. Pazdernik, *Langmuir* 13 (1997) 264–276.
- [29] R.C. Hayward, A. Saville, A. Aksay, *Nature (London)* 404 (2000) 56–59.
- [30] N. Denkov, O. Velev, P. Kralchevski, I. Ivanov, H. Yoshimura, K. Nagayama, *Langmuir* 8 (1992) 3183–3190.
- [31] G. Bar, S. Rubin, R.W. Cutts, T.N. Taylor, T.A. Zawodzinski Jr., *Langmuir* 12 (1996) 1172–1179.
- [32] T. Sato, D.G. Hasko, H. Ahmed, *J. Vac. Sci. Technol., B: Microelectron. Nanometer Struct.* 15 (1997) 45–48.
- [33] T. Serizawa, H. Takeshita, M. Akashi, *Langmuir* 14 (1998) 4088–4094.
- [34] M. Himmelhaus, H. Takei, *Phys. Chem. Chem. Phys.* 4 (2002) 496–506.
- [35] N. Malikova, I. Pastoriza-Santos, M. Schierhorn, N.A. Kotov, L.M. Liz-Marzan, *Langmuir* 18 (2002) 3694–3697.
- [36] T. Taniguchi, S. Shinohara, S. Kawaguchi, K. Nagai, *Chem. Lett. (Japan)* (2002) 1180–1181.
- [37] G. Decher, J.-D. Hong, *Makromol. Chem. Macromol. Symp.* 46 (1991) 321–327.
- [38] G. Decher, J.-D. Hong, *Ber. Bunsen-Ges. Phys. Chem. Chem. Phys.* 95 (1991) 1430–1434.
- [39] G. Decher, *Science* 277 (1997) 1232.
- [40] P.T. Hammond, *Curr. Opin. Colloid Interface Sci.* 4 (2000) 430–442 (volume date 1999).
- [41] P. Bertrand, A. Jonas, A. Laschewsky, R. Legras, *Macromol. Rapid Commun.* 21 (2000) 319–348.
- [42] P. Chodanowski, S. Stoll, *J. Chem. Phys.* 115 (2001) 4951–4960.
- [43] F. Caruso, H. Lichtenfeld, E. Donath, H. Mohwald, *Macromolecules* 32 (1999) 2317–2328.
- [44] J.-A. He, R. Valluzzi, K. Yang, T. Dolukhanyan, C. Sung, J. Kumar, S.K. Tripathy, L. Samuelson, L. Balogh, D.A. Tomalia, *Chem. Mater.* 11 (1999) 3268–3274.
- [45] P. Welch, M. Muthukumar, *Macromolecules* 33 (2000) 6159–6167.
- [46] A.J. Khopade, F. Caruso, *Langmuir* 18 (2002) 7669–7676.
- [47] N. Kohli, P.R. Dvornic, S.N. Kaganove, R.M. Worden, I. Lee, *Macromol. Rapid Commun.* 25 (2004) 935–941.
- [48] Y. Lvov, K. Ariga, I. Ichinose, T. Kunitake, *J. Am. Chem. Soc.* 117 (1995) 6117–6123.

- [49] C. Picart, G. Ladam, B. Senger, J.C. Voegel, P. Schaaf, F.J.G. Cuisinier, C. Gergely, *J. Chem. Phys.* 115 (2001) 1086–1094.
- [50] N. Jessel, F. Atalar, P. Lavalle, J. Mutterer, G. Decher, P. Schaaf, J.C. Voegel, J. Ogier, *Adv. Mater.* 15 (2003) 692–695.
- [51] S. Kidambi, C. Chan, I. Lee, *J. Am. Chem. Soc.* 126 (2004) 4697–4703.
- [52] N.A. Kotov, I. Dekany, J.H. Fendler, *J. Phys. Chem.* 99 (1995) 13065–13069.
- [53] Y. Lvov, K. Ariga, M. Onda, I. Ichinose, T. Kunitake, *Langmuir* 13 (1997) 6195–6203.
- [54] W. Schrof, S. Rozouvan, E. Van Keuren, D. Horn, J. Schmitt, G. Decher, *Adv. Mater. (Weinheim, Germany)* 10 (1998) 338–341.
- [55] F. Caruso, M. Spasova, V. Salgueirino-Maceira, L.M. Liz-Marzan, *Adv. Mater. (Weinheim, Germany)* 13 (2001) 1090–1094.
- [56] J.W. Ostrander, A.A. Mamedov, N.A. Kotov, *J. Am. Chem. Soc.* 123 (2001) 1101–1110.
- [57] T.C. Wang, R.E. Cohen, M.F. Rubner, *Adv. Mater.* 14 (2002) 1534–1537.
- [58] N.E. Cant, H.-L. Zhang, K. Critchley, T.A. Mykhalyk, G.R. Davies, S.D. Evans, *J. Phys. Chem. B* 107 (2003) 13557–13562.
- [59] N. Ferreyra, L. Coche-Guerente, J. Fatisson, M. Lopez Teijelo, P. Labbe, *Chem. Commun. (Cambridge, UK)* (2003) 2056–2057.
- [60] T.C. Wang, M.F. Rubner, R.E. Cohen, *Chem. Mater.* 15 (2003) 299–304.
- [61] S. Kidambi, J. Dai, J. Li, M.L. Bruening, *J. Am. Chem. Soc.* 126 (2004) 2658–2659.
- [62] P.A. Kralchevsky, K. Nagayama, *Langmuir* 10 (1994) 23–36.
- [63] S. Rakers, L.F. Chi, H. Fuchs, *Langmuir* 13 (1997) 7121–7124.
- [64] M. Barnsley, *Fractals Everywhere*, Academic Press Inc., Boston, 1988 (Chapter 5).
- [66] M. Semmler, E.K. Mann, J. Ricka, M. Borkovec, *Langmuir* 14 (1998) 5127–5132.
- [67] F.M. Horn, W. Richtering, J. Bergenholtz, N. Willenbacher, N.J. Wagner, *J. Colloid Interface Sci.* 225 (2000) 166–178.
- [68] E.L. Hinrichsen, J. Feder, T. Jossang, *Phys. Rev. Lett.* 44 (1986) 793.
- [69] J. Feder, *J. Theor. Biol.* 87 (1980) 237.
- [70] P. Meakin, *Annu. Rev. Phys. Chem.* 39 (1988) 237–267.
- [71] M. Lattuada, H. Wu, M. Morbidelli, *J. Colloid Interface Sci.* 268 (2003) 106–120.
- [72] P.C. Hiemenz, R. Rajagopalan, *Principles of Colloid and Surface Chemistry*, third ed., Marcel Dekker, New York, 1997.
- [73] I. Lee, J.S. Ahn, T.R. Hendricks, M.F. Rubner, P.T. Hammond, *Langmuir* 20 (2004) 2478–2483.
- [74] M.Y. Lin, H.M. Lindsay, D.A. Weitz, R.C. Ball, R. Klein, P. Meakin, *Nature* 339 (1989) 360–362.
- [75] I.M. Krieger, F.M. O'Neill, *J. Am. Chem. Soc.* 90 (1968) 3114–3120.
- [76] M. Born, E. Wolf, *Principles of Optics: Electromagnetics Theory of Propagation Interference and Diffraction of Light*, fourth ed., Pergamon, Oxford, 1970.
- [77] S. Walheim, E. Schaffer, J. Mlynek, U. Steiner, *Science (Washington, DC)* 283 (1999) 520–522.
- [78] G.A. Neuman, P.I.I. Glass Technology Center, Pittsburgh, PA, USA, *J. Non-Cryst. Solids* 218 (1997) 92–99.
- [79] J. Szczyrbowski, G. Braeuer, G. Teschner, A. Zmely, W.-R.-S. Leybold Systems GmbH, Hanau, Germany, *J. Non-Cryst. Solids* 218 (1997) 25–29.
- [80] J. Hiller, J.D. Mendelsohn, M.F. Rubner, *Nat. Mater.* 1 (2002) 59–63.
- [81] Y. Yagi, S.I. Matsushita, D.A. Tryk, T. Koda, A. Fujishima, *Langmuir* 16 (2000) 1180–1184.
- [82] T.C. Wang, B. Chen, M.F. Rubner, R.E. Cohen, *Langmuir* 17 (2001) 6610–6615.
- [83] S.Y. Yang, J.D. Mendelsohn, M.F. Rubner, *Biomacromolecules* 4 (2003) 987–994.